Tailoring calcium-alginate hydrogels: a systematic study of molecular weight and concentration effects

International Journal of Biological Macromolecules 357 (2026) 151578

Contents lists available at ScienceDirect

International Journal of Biological Macromolecules

journal homepage: www.elsevier.com/locate/ijbiomac

Tailoring calcium-alginate hydrogels: a systematic study of molecular weight and concentration effects

Sabrina Cuomo [a], Francesca Rispo [a], Bartolomeo Coppola [b], Emiliano Bedini [c], Maria D'Agostino [a], Elisabetta Cassese [a], Paola Palmero [b], Chiara Schiraldi [a], Annalisa La Gatta [a,*]

[a] Department of Experimental Medicine, School of Medicine, University of Campania "Luigi Vanvitelli", Via L. De Crecchio 7, 80138, Napoli, Italy
[b] Politecnico di Torino, Department of Applied Science and Technology, INSTM R.U. Lince Laboratory, Corso Duca Degli Abruzzi, 24, Italy
[c] Department of Chemical Sciences, University of Naples Federico II, Complesso Universitario Monte S.Angelo, via Cintia 4, I-80126, Napoli, Italy

ARTICLE INFO

Keywords:
Alginate
Hydrodynamic analysis
Hydrogel
Ionic-crosslinking
Concentration
Molecular weight
Human dermal fibroblasts

ABSTRACT

Calcium-Alginate (Ca-Alg) hydrogels with tunable properties are increasingly desired across diverse applications, yet our understanding of how their structure–property relationships determine performance remains limited. Here, we systematically examined alginate molecular weight (M_w) and concentration (c) as key levers to modulate Ca-Alg hydrogel behaviour.

Three alginates, spanning low to high viscosity, were fully characterized by Size-Exclusion Chromatography–Triple-Detector-Array (SEC-TDA), revealing distinct molecular weight distributions (M_w 123 ± 4 to 400 ± 20 kDa; M_w/M_n = 1.5–2.3). Ca-Alg hydrogel sponges were fabricated from these alginates at 10–40 g/L concentrations, and the impact of M_w and c on their properties was assessed. Polymer concentration primarily influenced sponge density, while the the 3D-microarchitecture became increasingly well-defined with M_w and c. Apparent porosity remained consistently high (>90%), whereas water-uptake (4–7 g/g) exhibited limited and inconsistent dependence on the parameters. In contrast, mechanical stiffness and degradation kinetics, two critical determinants of hydrogel performance, were strongly and predictably enhanced by higher M_w and c with G′ values in the range 4–260 kPa and residual mass after 30 days in Phosphate-Buffer-Saline varying from about 23% to 66%. Quantitative relationships correlating these properties to polymer chain-length and concentration were established, providing a predictive framework for rational hydrogel design.

Biological evaluation demonstrated comparable human dermal fibroblast colonization, proliferation, and collagen-I expression in sponges with the most divergent physicochemical characteristics.

Overall, these results offer valuable insights into the roles of alginate M_w and concentration in determining Ca-Alg hydrogel performance and provide mathematical correlations to guide optimization toward targeted applications.

1. Introduction

Sodium alginate (Alg) is a naturally abundant marine polysaccharide primarily extracted from brown seaweeds (*e.g.*, *Laminaria hyperborea*, *Macrocystis pyrifera*) or produced *via* bacterial fermentation (*e.g.*, *Azotobacter*, *Pseudomonas aeruginosa*) [1–3]. It is a linear copolymer composed of β-D-mannuronic acid (M) and α-L-guluronic acid (G) residues linked by 1,4-glycosidic bonds, arranged in homopolymeric (MMM or GGG) and heteropolymeric (MGMG) blocks. The M/G ratio varies depending on the alginate source and influences its macromolecular properties [4,5].

Thanks to its biocompatibility, biodegradability, and low cost, alginate is widely employed in biomedical, biotechnological, and food applications, primarily in the form of hydrogel. Among various crosslinking methods, calcium ion-induced gelation (Alg–Ca hydrogels) is the most common, as it occurs under mild conditions and avoids the use of toxic solvents [6].

Alg–Ca hydrogels are versatile materials used in wound dressings, tissue engineering scaffolds, probiotic encapsulation, drug delivery, and food preservation [7–18]. Features such as porosity, water uptake capacity, rheological behaviour, and stability in physiological environments critically influence hydrogel performance by affecting drug

* Corresponding author.
E-mail address: annalisa.lagatta@unicampania.it (A. La Gatta).

https://doi.org/10.1016/j.ijbiomac.2026.151578
Received 16 December 2025; Received in revised form 10 March 2026; Accepted 19 March 2026
Available online 20 March 2026

release profiles, cell behaviour, including adhesion, proliferation, and differentiation (particularly in stem cell-based tissue engineering), and long-term *in vivo* functionality. [6–8,10,16,19–22].

Given the significant scientific, clinical, and commercial interest in Alg–Ca hydrogels, enhancing our ability to fine-tune their physicochemical and mechanical properties to match the requirements of specific applications is therefore highly desirable [4,23–25]. Beyond established factors such as the Ca/Alg ratio and the mannuronic-to-guluronic acid (M/G) ratio, both the molecular weight distribution of alginate and its concentration in calcium-containing crosslinking solutions are known to influence hydrogel characteristics [19,26]. However, to the best of our knowledge, these parameters have been only partially and rarely investigated in a systematic manner. Although some studies have explored the effect of alginate concentration on the properties of Alg–Ca hydrogels [3,6–8,20,22,27–31], they present several limitations: they often focus on a limited subset of parameters, do not analyse quantitative or mathematical relationships, and rarely provide adequate and thorough characterization of the alginate samples, limiting reproducibility and broader applicability.

On the other hand, few studies have investigated the impact of alginate molecular weight on the properties of its calcium hydrogels with detailed Mw characterization, most of them considering molecular weight only indirectly through viscosity grades [8,32,33]. This gap largely stems from the challenges in obtaining detailed molecular weight distribution data for these polymeric samples. In fact, manufacturers typically provide only indirect information, classifying alginate samples as “low,” “medium,” or “high” viscosity based on the viscosity of a 1 wt% aqueous polymer solution. Moreover, the technology required for accurate characterization of naturally occurring polydisperse polymers remains limited in accessibility. To the best of the authors' knowledge, only Gong and colleagues have examined the effect of alginate molecular weight on Ca–Alg hydrogels, but their focus was limited to its influence on the polymer's membrane-forming ability [22].

Taken together, these limitations highlight the need for a systematic investigation in which alginate molecular weight distribution is rigorously characterized and correlated, together with polymer concentration, with hydrogel properties.

On this basis, the present study aimed to gain a broader, deeper, and more reliable understanding of the correlation between alginate molecular weight (M_w) and concentration (c), and the performance of Ca-Alg hydrogels. To this end, three commercial alginate samples (high, medium, and low viscosity), all from the same supplier (Thermo Fisher), were fully characterized hydrodynamically using the state-of-the-art technique (SEC-TDA), providing a comprehensive description of their molecular weight distributions, including conformational information.

These samples were subsequently used to prepare hydrogels as microporous sponges *via* ionic crosslinking with calcium ions, investigating alginate concentrations ranging from 10 to 40 g/L. The resulting hydrogels were characterized for features that are considered critical to most alginate applications, particularly biomedical ones, including density, porosity, microarchitecture, hydration, rheological properties, and stability under physiological conditions. Potential mathematical correlations between the quantified biophysical parameters and the molecular weight and concentration of the polymer subjected to crosslinking were also investigated.

Based on the study design, we expected to broaden the current understanding of Alg-Ca hydrogels by providing deeper insights into whether, and how, alginate molecular weight and concentration can be leveraged to fine-tune hydrogel performance, thereby optimizing their use and expanding their potential applications.

2. Materials and methods

2.1. Materials

Five commercial-grade sodium alginate samples were used without further purification. Three of them, low viscosity (LV), medium viscosity (MV), and high viscosity (HV) alginic acid sodium salt (CAS Number: 9005-38-3) were purchased from Thermo Fisher Scientific (Kandel, Germany). Additional LV and MV alginic acid sodium salt samples were obtained from Sigma-Aldrich (St. Louis, MO, USA).

Dulbecco's phosphate buffered saline without calcium and magnesium (PBS) was purchased from Termo Fisher Scientific. Sodium nitrate ($NaNO_3$) (CAS Number: 7631-99-4), sodium azide (NaN_3) (CAS Number: 26628-22-8) and acetone (CAS Number 67-64-1) were purchased from Sigma-Aldrich Chemicals Co. (St. Louis, MO). Calcium chloride dihydrate ($CaCl_2{\cdot}2H_2O$) (CAS Number: 10035-04-8) analytical grade, was purchased from Titolchimica s.p.a (Italy). Ethanol (≥99%) (CAS Number: 64-17-5) was purchased from Fischer Scientific (UK). Purified water was used throughout and was obtained using a Millipore Milli-Q water System.

For the biological experimentation, Human dermal Fibroblasts cell line (HDF), immortalized with hTERT (HDF cells, BJ-5ta, ATCC CRL-4001) were used.

All reagents for cell culturing were obtained from GIBCO (Thermo Fisher Scientific, Waltham, MA, USA) phenol red-free Dulbecco's Modified Eagle Medium (DMEM), Heat inactivated fetal bovine serum (FBS), penicillin-streptomycin and fungizone (CAS Number: 1397-89-3).

MTT (3-(4,5-dimethylthiazol-2-yl)-2,5-diphenyltetrazolium bromide) (CAS Number:

298-93-1), Trizol solution, Reverse Transcription System Kit, were purchased from Thermo Fisher ScientificIQ ™ SYBR® Green Supermix was obtained from (Bio-Rad Laboratories, Milan, Italy).

2.2. SEC-TDA characterization

The hydrodynamic characterization of the alginate samples was accomplished using a Size Exclusion Chromatography–Triple Detector Array (SEC–TDA) system (Viscotek, Malvern, UK). A detailed description of the system is reported elsewhere [34].

Briefly, the setup consisted of two main 1components: the GPCmax VE 2001 integrated system, including a gel permeation chromatography pump, in-line solvent degasser, and autosampler; the TDA302 triple detector array module, equipped with a column oven, refractive index (RI) detector, viscometer, and both right-angle (RALS) and low-angle (LALS) light scattering detectors. The light scattering system is optimized for signal-to-noise ratio, with measurements performed at a 7° angle from the incident beam. Two TSK–GEL GMPWXL columns were used in series (Tosoh Bioscience, Italy; Cat. No. 8–08025; hydroxylated polymethacrylate, 100–1000 Å pore size, 13 μm particle size, 7.8 × 30.0 cm), preceded by a guard column (Cat. No. 08033; 12 μm particle size, 6.0 × 4.0 cm).

Alginate samples were initially dissolved in deionized water at a concentration of 10 g/L, then opportunely diluted for analysis (final column load between 0.2 and 0.4 dL). Prior to injection, samples were filtered through 0.22 μm disposable syringe filters.

Analyses were performed under isocratic conditions using a 0.1 M $NaNO_3$ aqueous solution (pH 7.0) as the mobile phase, at a flow rate of 0.6 mL/min, at 40 °C, over a 1-hour run.

Data were acquired and processed using OmniSEC software (Malvern Instruments). A dn/dc value of 0.165 was used [35]. The following parameters were determined: weight-average molecular weight (M_w), number-average molecular weight (M_n), polydispersity index (M_w/M_n), hydrodynamic radius (R_h), intrinsic viscosity (η), Mark–Houwink parameters (log k and a). Additionally, the sample fraction (wt%) exhibiting M_w higher than 300 kDa was also derived.

2.3. ^1H NMR analyses

^1H NMR liquid-state NMR spectra were recorded in D_2O at 298 K on a Bruker Avance III HD 600 MHz spectrometer (Billerica, MA, USA) equipped with a cryo-probe (^1H: 600 MHz, acetone as internal standard

at 2.22 ppm for spectra in D_2O), using a Bruker TopSpin 4.0.5 software for data analysis.

2.4. Hydrogel preparation

Ca-Alg hydrogels were prepared following the method described by Gong et al. [22], with some modifications. The procedure is schematized in Fig. 1.

Briefly, each sodium alginate sample was dissolved at the desired concentration (10, 20, 30, and 40 g/L) in deionized water. The resulting solutions were centrifuged at 6000*g* for 10 min to remove air bubbles. 5 mL of each solution were carefully poured into Teflon plates (0.128 mL/cm^2), frozen at −20 °C for 3 h, and subsequently lyophilized using an EPSILON 2-6D lyophilizer (Christ, Germany) according to a program consisting of two stages: 1) RT, 1 mbar (16–17 h); 2) RT, 0.1 mbar (2 h).

The resulting dry sponge samples were peeled off the plates and crosslinked by immersion in 10 mL of 5 wt% $CaCl_2$ aqueous solution (ensuring a molar excess of calcium ions relative to alginate carboxylates regardless of the initial alginate concentration) under stirring at 30 rpm for 3 h.

After crosslinking, samples were purified by washing with deionized water until the conductivity of the wash water stabilized. The purified hydrogels were then frozen again at −20 °C for 3 h and subjected to a second freeze-drying cycle to ensure complete water removal (Fig. 1).

Resulting hydrogels will be referred to as XLV-y, XMV-y, and XHV-y, where "y" denotes the alginate concentration (g/L) used in the preparation.

2.5. Hydrogel morphological analyses

For the observation of sample surfaces (top and side), the XAlg samples, as resulting from the procedure described in the previous paragraph, were directly sputter-coated with a platinum–palladium layer (Denton Vacuum Desk V sputter coater, USA), mounted on stubs, and observed using a Supra 40 Zeiss scanning electron microscope operated at 5 kV with an InLens detector. Imaging was performed using Smart SEM Zeiss software. Cross-sectional morphology was assessed through cryogenic fracturing. Samples were immersed in liquid nitrogen (LN_2) for 5 min and then fractured rapidly to produce a brittle fracture. Fracture surfaces were then sputtered with platinum and observed using Field Emission Scanning Electron Microscopy (FESEM - Hitachi, Tokyo, Japan).

Pore size was determined by image analysis using a commercial software (Scandium by Soft Image System). The analysis of pore size was made using FESEM micrographs with different magnifications; an average of 150 pores for each concentration was measured.

2.6. Hydrogel dimensions, density and porosity

The dimensions, density, and porosity of the sponges were evaluated following previously reported methods for hydrogels, with some modifications, focusing on the samples with the lowest and highest alginate concentrations for each molecular weight [36]. The sponges were cylindrically shaped. Their diameter was measured using a ruler. Sample thickness was determined using a Physica rotational rheometer (MCR 301, Anton Paar, Germany), which allows for the measurement of sample thickness while monitoring the force applied to the sample. Briefly, a parallel plate geometry was used: after setting the zero gap, the sample was placed on the lower plate, and the upper plate was lowered until a force between 0.2 and 0.5 N was detected, indicating contact with the sponge surface. The corresponding gap was recorded as the sponge thickness. For each X-Alginate sponge, three replicates were measured, and each replicate was measured three times. The mean thickness value of each replicate was used to calculate the sponge volume (V_t). The latter was calculated considering the cylindrical shape, as the product of the base area and the measured thickness.

Sponge apparent (or geometrical) density was calculated as the ratio between the sponge mass (w_0), measured with an analytical balance (Mettler-Toledo, XS105 DualRange), and the sponge apparent volume (V_t).

Sponge porosity was calculated according to Eq. (1):

$$\text{porosity}\ (\%) = (V_v/V_t) \times 100 \tag{1}$$

where V_v = sponge void volume; V_t = sponge apparent volume the sponge void volume V_v was evaluated by means of the liquid displacement method as already reported with modifications [37]. Specifically, each dry sponge was weighed (w_0), immersed in absolute ethanol and left to saturate under vacuum to ensure the pores were completely filled. Then, the weight of saturated samples was determined (w_h).

The void volume was calculated according to the Eq. (2):

$$V_v = (w_h - w_0)/\rho_e \tag{2}$$

where ρ_e was ethanol density.

Measurements were carried out at least in triplicate and results reported as the mean value ± SD.

2.7. Swelling studies

The water uptake ability of the X-Alginate samples was evaluated by gravimetric measurements using an analytical balance (Mettler Toledo, XS105 Dual Range, Novate Milanese, Italy), following previously described methods for similar hydrogels [36]. Briefly, dry samples were weighed (w_0) and placed in sterile containers to swell to equilibrium in either distilled water or PBS solution. The samples were then carefully removed, surface water was quickly blotted with filter paper, and the swollen weight (w_s) was recorded.

The swelling ratio (g/g) was calculated using Eq. (3):

$$\textit{swelling ratio}\ (g/g) = w_s/w_0 \tag{3}$$

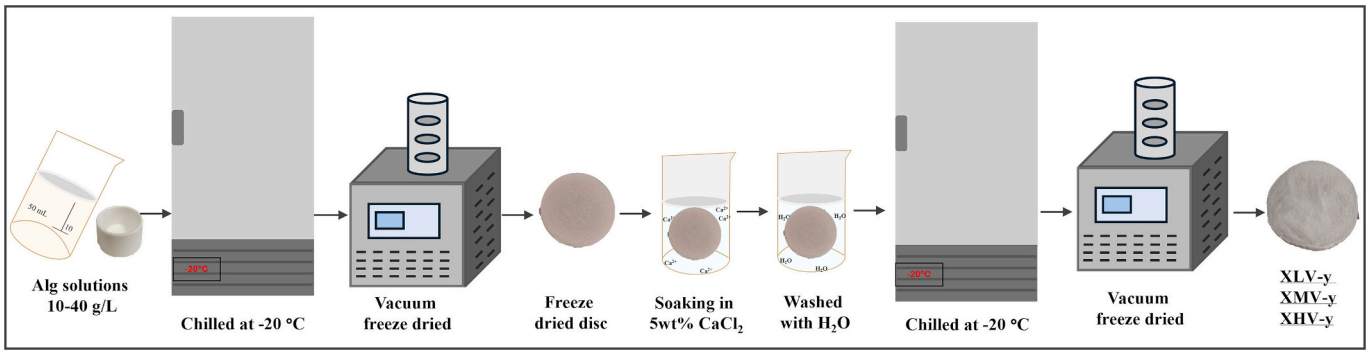

Fig. 1. Schematic representation of the preparation process of XAlg sponges.

where w_s = swollen sample weight; w_0 = dry (initial) sample weight.

Experiments were carried out at least in triplicate and results were reported as the mean value ± SD.

2.8. Hydrogel rheological behaviour

Rheological measurements were performed using a Physica MCR301 oscillatory rheometer (Anton Paar, Germany) equipped with a parallel plate geometry (25 mm diameter) and Peltier temperature control.

All measurements were conducted on sponge samples previously equilibrated in physiological medium at 37 °C. Care was taken to maintain full sample hydration throughout the measurements.

A strain sweep test was first performed over a strain range of 0.001–100% at a constant frequency of 1.59 Hz, in order to identify the Linear Viscoelastic Region (LVR). Within this range, the storage modulus (G′) and the loss factor (tan δ) were recorded. Subsequently, a frequency sweep test was conducted over the range of 0.159–15 Hz, using a strain value previously identified within the LVR. Mechanical spectra were recorded.

2.9. Hydrogel degradation under physiological conditions

To assess hydrogel degradation under physiological conditions, weighed X-Alg samples (m_1) were placed in sterile containers, added with 2 mL of PBS and incubated at 37 °C for 30 days in a thermomixer (Eppendorf, USA) under stirring (300 rpm). At the end of the incubation period, the samples were collected, rinsed thoroughly with deionized water (ddH_2O), and the conductivity of the wash solution was measured to ensure complete removal of residual salts. The washed samples were then freeze-dried and further dried overnight in a vacuum oven at 40 °C.

Finally, the dried samples were weighed (m_2), and the sensitivity to degradation under the tested conditions was evaluated by calculating the sample residual mass (%) according to Eq. (4):

$$\text{Residual mass}\ (\%) = [m_2/m_1] \times 100 \tag{4}$$

2.10. Human dermal fibroblasts culture

Human Dermal Fibroblasts (HDFs) were cultivated in phenol red-free Dulbecco's Modified Eagle Medium (DMEM) supplemented with 10% (*v*/v) heat inactivated fetal bovine serum (FBS), 100 U/mL penicillin and 100 μg/mL streptomycin and fungizone 2.5 μg/mL.

2.10.1. Human dermal fibroblasts seeding and viability in the alginate sponges

XLV-10 and XHV-40 were selected to evaluate the response of human dermal fibroblasts (HDFs). The XAlg samples were placed in a 24-well plate and allowed to swell in an HDF suspension (0.6–1.2 × 10^6 cells/cm^3). After cell seeding, additional culture medium was carefully added, if needed, until the sample reached its maximum equilibrium swelling. HDFs were also seeded on standard tissue culture plates (5 × 10^4 cells/well) as a control. All samples were incubated under standard culture conditions (37 °C, 5% CO_2). Once cell adhesion was observed in the control group, 1 mL of fresh medium was added to each well. Constructs and controls were cultured for up to 10 days, with medium replaced every two days.

Cell viability was assessed at 48 h, 6 days, and 10 days using the MTT assay (3-(4,5-dimethylthiazol-2-yl)-2,5-diphenyltetrazolium bromide), following the manufacturer's instructions with specific adaptations for 3D hydrogel systems. At each time point, the culture medium was removed and replaced with 1 mL of MTT solution 0.5 mg/mL in culture medium without phenol red. Samples were incubated for 3 h to allow the formation of formazan crystals within viable cells. The MTT solution was then aspirated and replaced with 1 mL of 0.1 M HCl in isopropanol to solubilize the formazan. To achieve uniform diffusion throughout the hydrogel matrix, samples were stirred gently for 3 h. After MTT incubation and prior to solubilization, representative photographs of the hydrogel constructs were taken to qualitatively assess the distribution of the purple formazan staining within the matrix. These images provided visual evidence of the spatial distribution of metabolically active cells across the scaffold.

Absorbance was measured at 570 nm using a GloMax Discover System spectrophotometer (Promega) and normalized to the volume of medium. The cell proliferation index at each time point was calculated relative to the 48-hours value according to the following Eq. (5):

$$\textit{proliferation index}\ (t) = A_{570}\ (t)/A_{570}(48\text{h}) \tag{5}$$

2.11. Gene expression analyses of type I collagen (COL single bondI) mRNA analyses using qRT-PCR

After 5 days of *in vitro* culture in the 3D sponges and on standard culture plates (control), HDFs were harvested and lysed using TRIzol reagent for RNA isolation. Subsequently, complementary DNA (cDNA) was synthesized from the isolated RNA using the Reverse Transcription System Kit (Thermo Fisher) according to the manufacturer's instructions. Gene expression of Collagen type I was quantitatively analysed by real-time reverse transcription polymerase chain reaction (RT-qPCR). The reactions were performed in triplicate using IQ™ SYBR® Green Supermix (Bio-Rad Laboratories, Milan, Italy) on a CFX Duet Real-Time PCR System (Bio-Rad). The mRNA expression levels were normalized to glyceraldehyde-3-phosphate dehydrogenase (GAPDH) as the housekeeping gene.

Relative gene expression differences between cells grown on the biomaterials and the control were calculated using the ΔΔCt method (where ΔΔCt represents the difference in ΔCt between samples and control). Data are presented as normalized fold expression calculated by the 2ˆ−ΔΔCt method.

The specific primer sequences used for these analyses are reported in Table 1.

2.12. Statistical analyses

Experiments were carried out at least in triplicate. Data were statistically evaluated by running a student *t*-test for comparison of two data groups and One-way ANOVA tests followed by *post hoc* correction for multiple comparison. p values $\leq$ 0.05 accounted for statistical significance.

3. Results

3.1. SEC-TDA characterization

The results from the SEC-TDA analyses of the three Thermo Fisher alginates are reported in Fig. 2.

In particular, the overlay of the chromatographic profile (RI signal) is reported in Fig. 2 and the values for the hydrodynamic parameters, as derived from the SEC-TDA analysis, are reported in Table 2.

The three samples significantly differed for all the investigated parameters ($p < 0.05$) except, as expected, for the Mark–Houwink constants (*a* and *logk*).

LV-, MV- and HV- Alg exhibited M_w equal to 123 ± 4 kDa, 275 ± 27 kDa and 400 ± 20 kDa, respectively with MV and HV Alg showing comparable and rather narrow distributions (M_w/M_n = 1.5–1.6) and the LV sample presenting the largest distribution (M_w/M_n = 2.3).

Table 1
Primer sequences for the qRT-PCR.

Gene name (symbol)	PCR primer sequence 5′ → 3′
Type I collagen (*COL-I*)	CAGCCGCTTCACCTACAGC TTTTGTATTCAATCACTGTCTTGCC

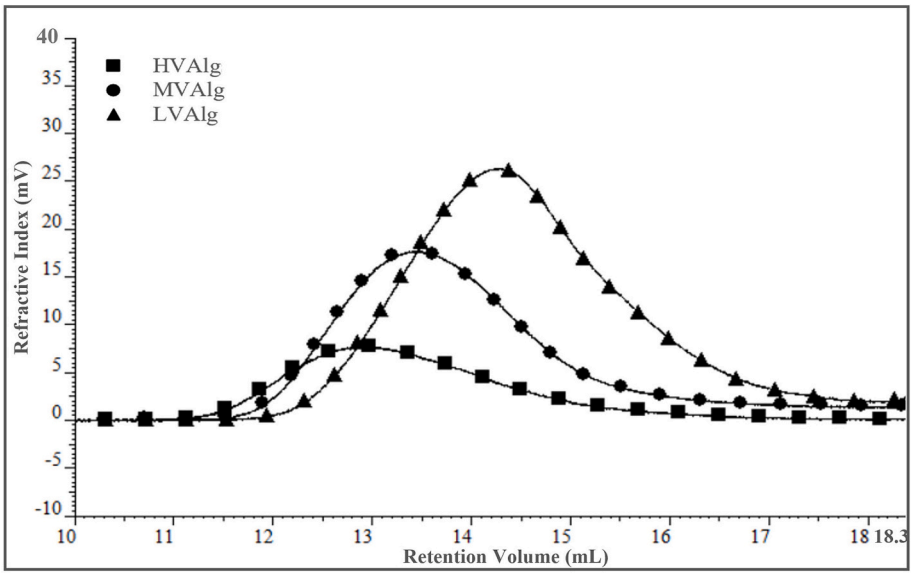

Fig. 2. Overlap of the SEC-TDA profiles (refractive index signal) for the three Alginate samples.

The intrinsic viscosity and hydrodynamic radius values increased consistently with the M_w, with values in the range of 5.6–15.1 dL/g and 21–44 nm, respectively.

The sample fraction (wt%) with M_w >300 kDa was 8 ± 1, 32 ± 1 and 58 ± 3 for LV, MV and HV Alg respectively.

A Low Viscosity and a Medium Viscosity- Alg by another supplier (Sigma Aldrich) were also analysed for comparison. The results from the SEC-TDA analyses for these latter samples are reported in Fig. 3. Specifically, the superimpositions of the RI profiles for the LV and MV Alg from the two suppliers are reported in Fig. 3. while the values for the hydrodynamic parameters are reported in Table 3.

The Sigma LV Alg exhibited M_w of 71 ± 9 kDa, with an intrinsic viscosity ([η]) of 2.6 ± 0.1 dL/g and a hydrodynamic radius (R_h) of 11.96 ± 0.02 nm. For the medium viscosity alginate, the molecular weight increases to 166 ± 29 kDa. Correspondingly, the intrinsic viscosity rises to 11.9 ± 0.2 dL/g, and the hydrodynamic radius (R_h) to 30 ± 2 nm. The sample fraction (wt%) values with M_w above 300 kDa were 27 ± 1 and 0 for the LV- and MV- sample, respectively.

The two Sigma samples differed significantly from each other in the investigated parameters. For both the low and the medium viscosity samples, significant differences were observed between the two suppliers in all the investigated parameters, with the exception of the Mark–Houwink constants (*a* and *logk*).

3.2. ^{1}H NMR analysis of the alginates

The analysis of the ^{1}H NMR spectra (Supplementary Information; Fig. S1 left) for the five alginate samples allowed to estimate their relative M/G and MM/MG/GG diad composition. In agreement with literature [38], the three peaks at 4.89–5.02, 4.50–4.64 and 4.31–4.43 ppm could be assigned to H-1 of M and G units and to H-5 of G residues.

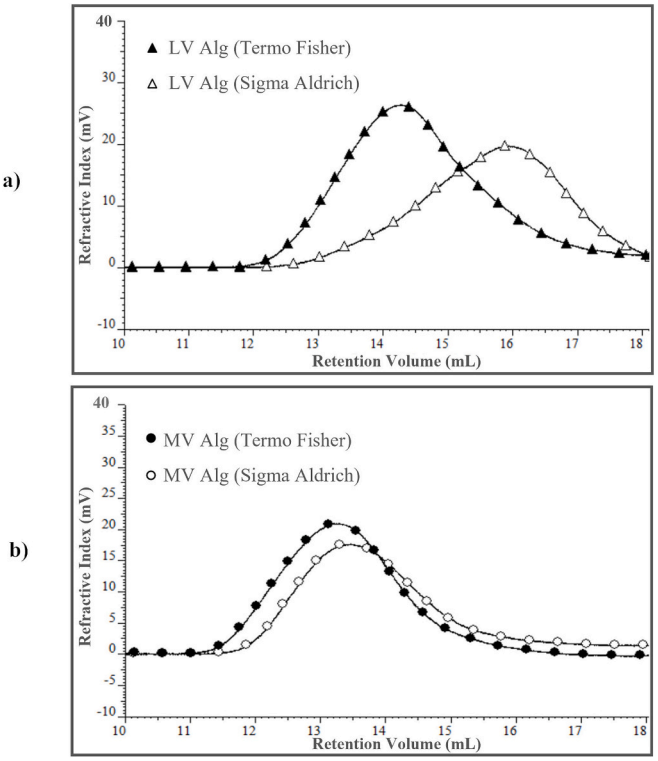

Fig. 3. Overlap of the SEC-TDA profiles (refractive index signal) of LV (a) and MV (b) alginates from Thermo Fisher and Sigma-Aldrich.

Table 2
Complete hydrodynamic parameters report for the LV-, MV- and HV-Alg samples (Thermofisher). Weight average molar mass (M_w), polydispersity index (M_w/M_n), intrinsic viscosity ([η]), hydrodynamic radius (R_h), sample fraction with M_w > 300 kDa (wt%), and Mark–Houwink constants (*a* and log *k*) are shown. Reported data are the mean ± SD of at least three replicates.

Alg sample	M_w (kDa)	M_w/M_n	[η] (dL/g)	R_h (nm)	Sample fraction with M_w >300 kDa (wt%)	a	logk
LV	123 ± 4	2.3 ± 0.3	5.6 ± 0.2	21 ± 1	8 ± 1	0.89 ± 0.01	−3.75 ± 0.04
MV	275 ± 27	1.6 ± 0.2	11.7 ± 0.2	35 ± 1	32 ± 1	0.95 ± 0.05	−4.1 ± 0.2
HV	400 ± 20	1.5 ± 0.2	15.1 ± 0.2	44 ± 1	58 ± 3	0.93 ± 0.04	−4.0 ± 0.2

Table 3
Complete hydrodynamic parameters report for the LV- and MV-Alg (Sigma-Aldrich): weight average molar mass (M_w), polydispersity index (M_w/M_n), intrinsic viscosity ([η]), hydrodynamic radius (R_h), sample fraction with M_w >300 kDa (wt%) and Mark–Houwink constants (*a* and log *k*) are shown. The analyses were carried out in triplicate and data are reported as the mean value ± SD.

Alg sample	M_w (kDa)	M_w/M_n	[η] (dL/g)	R_h (nm)	Sample fraction with M_w >300 kDa (wt%)	a	logk
LV	71 ± 9	4.1 ± 0.7	2.6 ± 0.1	11.96 ± 0.02	0	0.9 ± 0.1	−3.8 ± 0.4
MV	166 ± 29	1.2 ± 0.2	11.9 ± 0.2	30 ± 2	27 ± 1	0.9 ± 0.2	−3.8 ± 0.2

In particular, it is not possible to distinguish the chemical shift of anomeric hydrogens of G units in GG or GM sequences, as they resonate both in the region between 4.89 and 5.02 ppm. Similarly, the anomeric hydrogen atom of M units can be found at 4.50–4.64 ppm in the case of both MG and MM diads. Conversely, the H-5 atom of G residues involved in GG dyads is up field shifted (4.31–4.43 ppm) and therefore its signal is clearly distinguishable from the same signal related to GM sequences (4.50–4.64 ppm). From a relative integration of the three chemical shift regions indicated above (Supplementary Information; Fig. S2 right) and by applying the equations indicated in Table 4, it was possible to estimate the relative amount of M and G units composing the alginate backbone as well as their distribution in the relative diad sequences (Table 4).

3.3. Characterization of the XAlg sponges

3.3.1. Extent of alginate insolubilization, dimensions, density, morphology and porosity

Alginate (Alg) sponges exhibited similar macroscopic appearances following crosslinking and purification, regardless of the specific alginate type used (low, medium or high viscosity) or its initial concentration. Representative images of the crosslinked sponges are shown in Fig. 4a.

For all crosslinked alginate (XAlg) samples, the final mass after purification was comparable to the initial dry mass before crosslinking. This indicates that the crosslinking procedure was effective in fully insolubilizing the polymer, leaving no residual water-soluble fractions that could be lost during purification.

For each alginate type, sponges prepared from the lowest (10 g/L) and highest (40 g/L) concentrations were analysed for thickness, diameter, volume, apparent density, and porosity. The results are presented in Fig. 4b and c.

While the diameters remained consistent across samples, notable differences were observed in thickness, and consequently in volume and density, between the 10 g/L and 40 g/L sponges.

Specifically, the 40 g/L sponges exhibited thicknesses ranging from 0.45 to 0.47 cm and densities between 0.05 and 0.06 g/cm^3, with no significant differences among the three viscosity types (the three molecular weights). In contrast, the 10 g/L sponges displayed significantly reduced thicknesses (0.19–0.32 cm) and densities (0.02–0.04 g/cm^3). Among the 10 g/L samples, the LV sponge had the lowest thickness and volume, and consequently the highest density.

All samples demonstrated high porosity, ranging from 91% to 97%, with no statistically significant differences among them. Representative SEM and FESEM images are shown in Fig. 5. The images confirm the highly porous structure of the XAlg sponges. The 40 g/L samples exhibited a more uniform porous architecture, while the 10 g/L samples showed a more collapsed morphology, particularly at the top (a) and side (c) surfaces. In cross-section (b), the 10 g/L samples appeared to have larger pores, though fewer in number. Specifically, hydrogels prepared with a lower concentration (*i.e.* 10 g/L) exhibited pores in the range 60–473 μm, while those prepared with a higher concentration (*i.e.* 40 g/L) have smaller pores with a narrower distribution (27–269 μm). Moreover, the shape of the pores was also different, being more irregular in the sponges at lower concentrations, whereas it was more rounded and regular in the hydrogels at the highest concentration investigated.

3.3.2. Swelling behaviour

The swelling behaviour of the samples is summarized in Fig. 6. Pictures of a representative sponge in its dry and swollen state are reported in Fig. 6a. Upon immersion in deionized water, the samples increased their dry weight by approximately 3.6 to 7.1-fold. The swelling ratios data are presented twice, in Fig. 6b and c, arranged differently to better highlight the effect of concentration (10–40 g/L) for each specific molecular weight (Fig. 6b), and the effect of the molecular weight (LV, MV, HV; 129–400 kDa) at each concentration (Fig. 6c).

Data in Fig. 6b indicated that, for XLV and XMV, concentration did not significantly affect swelling, while XHV hydrogels swelled significantly more at 30 and 40 g/L than at 10 and 20 g/L ($p < 0.05$). However, no robust mathematical correlation could be found between hydrogels swelling and Alg concentration ($R^2 < 0.96$).

For the XAlg-10 and XAlg-20 samples (Fig. 6c), no significant

Table 4
Relative M/G and MM/MG/GG composition in the five commercially available Alg samples.

Alg sample	^{1}H NMR integrations				Composition		Diad composition	
	I_1[a]	I_2[b]	I_3[c]	%M[d]	%G[e]	%GG[f]	%GM=%MG[g]	%MM[h]
LV*	1.00	1.32	0.59	48%	52%	31%	21%	27%
MV*	1.00	1.61	0.42	51%	49%	21%	28%	23%
HV*	1.00	1.16	0.55	42%	58%	32%	26%	16%
LV#	1.00	1.23	0.71	68%	32%	23%	9%	59%
MV#	1.00	1.56	0.46	50%	50%	23%	27%	23%

[a] Relative integration of the 4.89–5.02 ppm region in the ^{1}H NMR spectrum.
[b] Relative integration of the 4.50–4.64 ppm region in the ^{1}H NMR spectrum.
[c] Relative integration of the 4.31–4.43 ppm region in the ^{1}H NMR spectrum.
[d] Evaluated according to the following Eq. (6): $\%M = I_2 - (I_1 - I_3)/I_1 + [I_2 - (I_1 - I_3)] \times 100$ (6).
[e] Evaluated according to the following Eq. (7): $\%G = 100 - \%M$ (7).
[f] Evaluated according to the following Eq. (8): $\%GG = I_3 \times \%G$ (8).
[g] Evaluated according to the following Eq. (9): $\%GM = \%MG = (I_1 - I_3) \times \%G$ (9).
[h] Evaluated according to the following Eq. (10): $\%MM = 100 - [\%GG - (2 \times \%GM)]$ (10).
* Thermo Fisher Alg.
# Sigma Aldrich Alg.

a)

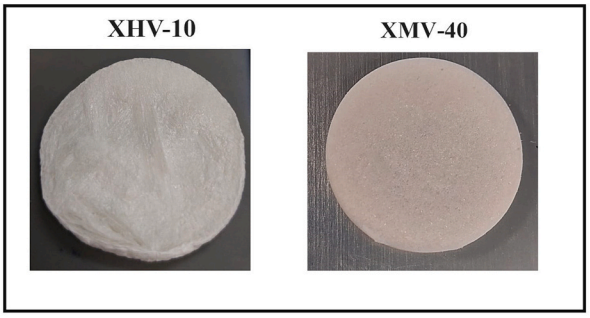

b)

Sample	Thickness (cm)	Diameter (cm)	Volume (cm^3)
XHV-40	0.47 ± 0.01	3.2 ± 0.1	3.9 ± 0.3
XHV-10	0.32 ± 0.02	3.0 ± 0.3	2.3 ± 0.5
XMV-40	0.45 ± 0.01	3.2 ± 0.03	3.9 ± 0.1
XMV-10	0.29 ± 0.01	3.1 ± 0.05	2.4 ± 0.1
XLV-40	0.47 ± 0.05	3.1 ± 0.2	3.5 ± 0.2
XLV-10	0.19 ± 0.03	3.1 ± 0.1	1.4 ± 0.2

c)

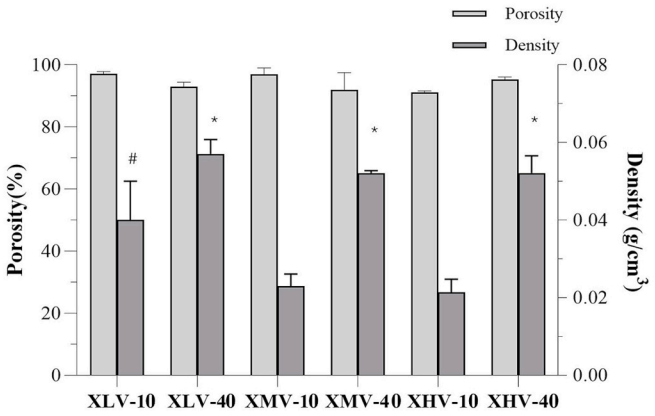

Fig. 4. a) Representative images of XAlg sponges; XHV-10 and XMV-40 samples are shown.
b) Sponge dimensions (thickness, diameter, and volume). Thickness and diameter were measured for 10 g/L and 40 g/L XAlg sponges at the end of the fabrication process; volume was estimated assuming a cylindrical geometry. c) Density and porosity of 10 g/L and 40 g/L XAlg sponges.
$^{\#}p < 0.01$ *vs* all other samples; *$p < 0.01$ *vs* XLV-10, XMV-10, and XHV-10.

differences in water uptake were observed when moving from the XLV (129 kDa) to the XHV (400 kDa) alginate. At higher concentrations (30 and 40 g/L), hydrogels with the highest molecular weight Alg (XHV) showed significantly higher water-uptake than those with lower M_w ($p < 0.01$ and $p < 0.05$, respectively). No robust mathematical correlation could be found even between hydrogels swelling and Alg M_w ($R^2 < 0.96$). In the present work, only correlations showing very high coefficients of determination were considered sufficiently robust to support predictive relationships between polymer molecular parameters and hydrogel properties.

The hydrogels water up-take ability was measured also in PBS, showing no significant difference compared to dd-water (Supplementary Information; Fig. S2).

3.3.3. *Rheological behaviour*

The results of the rheological studies are reported in Fig. 7. All the sponges exhibited behaviour typical of a crosslinked network, with storage modulus (G′) values consistently higher than loss modulus (G″), and only slight dependence on frequency. Representative mechanical spectra are shown in Fig. 7a.

The crosslinked sponges displayed a wide range of G′ values, from approximately 4 kPa up to 260 kPa. To better elucidate the influence of polymer concentration (*c*) and molecular weight (M_w) on hydrogel rigidity, G′ values are presented differently arranged in Fig. 7b (effect of concentration at each M_w) and Fig. 7c (effect of M_w at each concentration).

Data from Fig. 7b show that polymer concentration significantly affects hydrogel stiffness for each molecular weight. For XLV, XMV, and XHV alginates, G′ increased from 4 to 92 kPa, 11 to 190 kPa, and 23 to 259 kPa, respectively, as the concentration increased from 1 to 40 g/L. The G′ values for each molecular weight were well correlated with concentration (R^2 = 0.96–1.00), with G′ scaling exponentially with concentration as $G' \propto e^{mc}$, where m ~ 0.1. Specifically, $G' = 11e^{0.08c}$; $G' = 4\,e^{0.1c}$ and $G' = 2\,e^{0.1c}$, respectively for XLV, XMV and XHV, respectively.

Data from Fig. 7c clearly show that alginate molecular weight also strongly influences hydrogel rigidity at all tested concentrations. Specifically, at each concentration, the storage modulus increased linearly with M_w (R^2 = 0.96–0.99), with the effect becoming far more

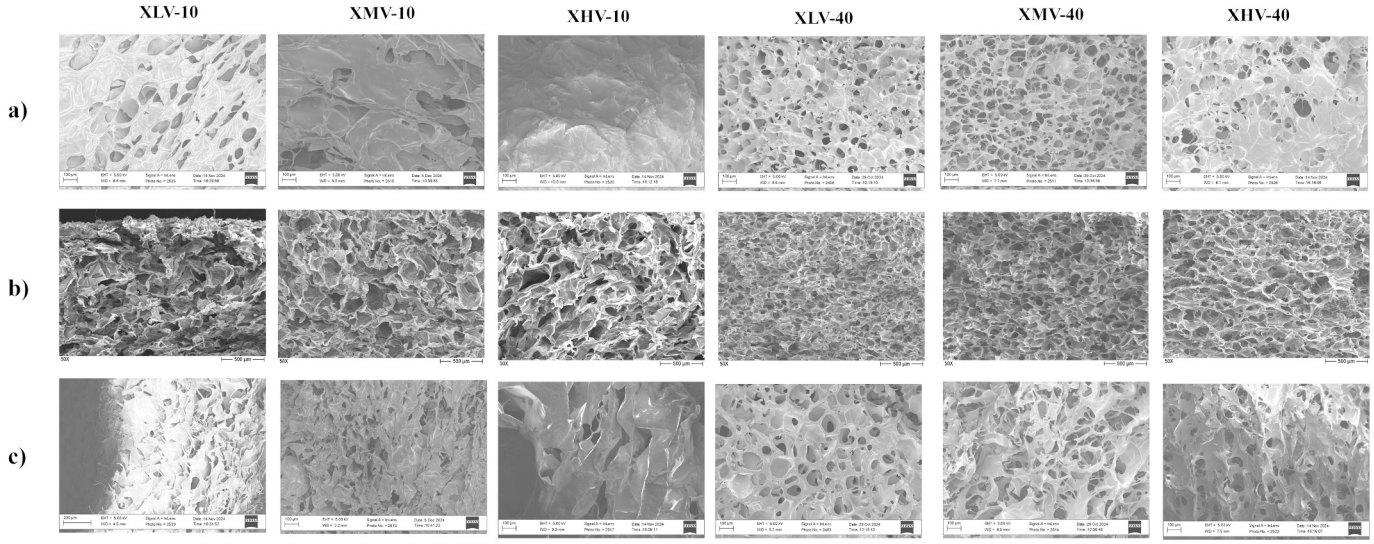

Fig. 5. Representative SEM (a, c) and FESEM (b) micrographs of XLV, XMV, and XHV samples (10–40 g/L): (a) top surface (200× magnification), (b) liquid nitrogen (LN_2) fracture cross-section (50× magnification), and (c) side surface (200× magnification).

pronounced at higher polymer concentrations ($G' = 0.7M_w$ for the 40 g/L X-Alg sponges *vs* $G' = 0.05M_w$ for the 10 g/L).

3.3.4. Stability under physiological conditions

Results of sample degradation in physiological medium are shown in Fig. 8. Specifically, the residual mass (wt%) of the specimens after 30 days of incubation in PBS at 37 °C is reported. To better highlight the effects of molecular weight (M_w) and concentration (*c*), data are again presented separately in Fig. 8a and b. The results clearly indicate that all samples progressively degraded under the tested conditions, albeit at different rates. Stability increased with both alginate concentration (Fig. 8a) and molecular weight (Fig. 8b), with residual mass (Rm) values ranging from 23 wt% (lowest polymer concentration and M_w) to 66 wt% (highest values of *c* and M_w). Sponge stability was well correlated with both alginate concentration and molecular weight, scaling logarithmically with both parameters. Specifically, Rm = 16ln(c)-13; Rm = 15ln(c)+3 and Rm = 20ln(c)-6 for XLV, XMV and XHV, respectively. When considering Rm as a function of Mw at the diverse tested concentrations, Rm was found = 14ln(Mw)-44 and Rm = 18ln(Mw)-44 for the lowest and the highest concentrations tested, respectively. A synergistic positive effect of these two factors on hydrogel stability can be inferred.

3.3.5. Response of HDFs to the XAlg sponges

The results of HDF viability within the XAlg sponges are presented in Fig. 9. Specifically, Fig. 9a shows representative images of XLV-10 and XHV-40 sponges at 48 h post-seeding and following incubation with the MTT solution. The presence of formazan crystals, produced exclusively by metabolically active cells, is clearly visible throughout the samples, suggesting a homogeneous distribution of viable cells within the bulk of the sponges.

Quantitative viability data are shown in Fig. 9b. The proliferative indices of HDFs cultured in the sponges (XLV-10 and XHV-40) and on tissue culture polystyrene (TCP), evaluated at days 6 and 10 *vs* day2, are reported. For all samples, a significant increase in cell viability was observed over time, indicating ongoing cell proliferation under each condition. Notably, while the proliferation rates were comparable between all groups from day 2 to day 6, a reduced proliferative capacity was observed in the sponge groups between days 6 and 10. Specifically, the proliferation index for HDFs cultured in the XAlg sponges was approximately 3 (with no significant difference between the two), compared to values exceeding 6 in the control (TCP) group.

Fig. 9c presents the results of RT-PCR analysis of ***COLI*** gene expression at day 6. Expression levels in cells cultured within the XAlg sponges were normalized to those of the TCP control. A marked down-regulation of COLIA1 expression was detected in both sponge types, with no significant differences between them, each exhibiting approximately 0.2-fold expression relative to the control.

4. Discussion

In an attempt to provide insights to guide and advance the design and optimization of Ca-Alg gels, the influence of alginate molecular weight (M_w) and concentration (c) on the key properties of the gels was systematically investigated.

Three commercially available alginate samples, labelled as “low-”, “medium-” and “high-viscosity” alginate were employed. The selected alginate concentrations (10–40 g/L) fall within the range commonly reported for Ca–alginate hydrogel preparation in biomedical applications. [7,8,11,22,39]. Hydrogels were produced in the form of microporous sponges which is a widely adopted 3D architecture in various applications, particularly in the biomedical field [7,8,20,22,27,39]. Attention was paid to minimize variations in parameters, other than those under investigation, that could affect the hydrogel behaviour. To this end, all alginate samples were sourced from giant brown seaweed (*Macrocystis pyrifera*) and crosslinking conditions were selected to ensure effective and reproducible network formation under otherwise identical conditions. In particular, a molar excess of calcium ions relative to alginate carboxylates and a crosslinking time sufficient to achieve complete polymer insolubilization were used. Moreover, although the M/G composition is a structural parameter that is inherently difficult to control, the ^{1}H NMR analyses showed a relatively narrow range (from 42:58 to 51:49) among the samples. Similarly, the percentage of GG blocks, a parameter critically influencing alginate gelling abilities and hydrogel properties, varied over a rather small range as well (from 21% to 32%). The observed structural variations among the three alginate samples indicate that their impact on the final hydrogel behaviour is likely to be limited.

As a key achievement of the study, the Alg samples were fully hydrodynamically characterized using the SEC-TDA system (Fig. 2; Table 2). The comprehensive set of hydrodynamic parameters obtained demonstrated significant differences in the molecular weight distribution, with M_w, intrinsic viscosity, and hydrodynamic radius values consistently (and significantly) increasing from the low-viscosity to the high-viscosity sample. These differences confirmed that the selected

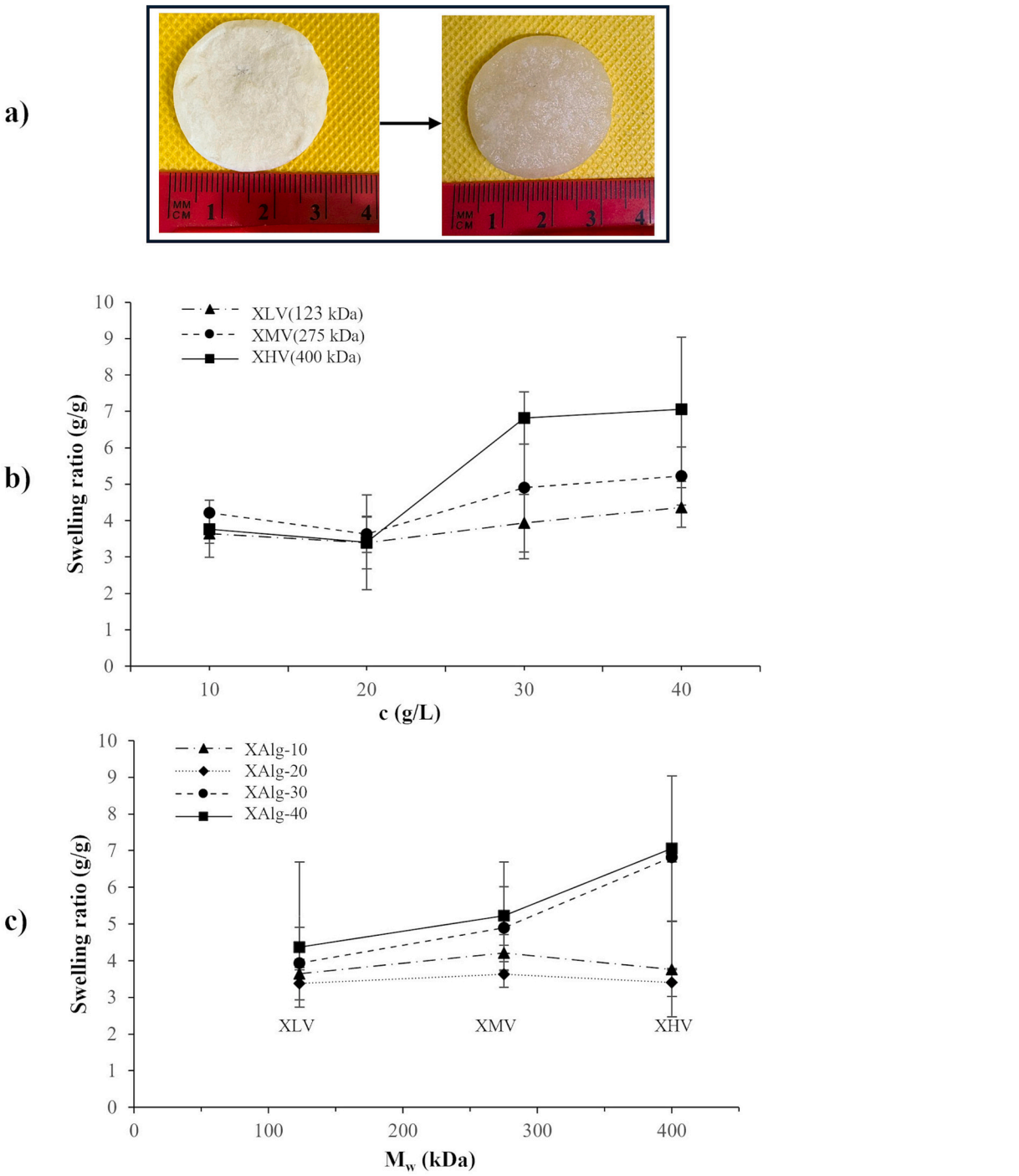

Fig. 6. Hydrogel swelling behaviour.
a) Representative images of an alginate sponge in the dry state (left) and after equilibration in physiological medium (right).
Swelling ratio values for the hydrogels at equilibrium at 37 °C, as a function of Alginate concentration (b) and as a function of Alginate M_w (c).

samples are well-suited for investigating how polymer chain length affects hydrogel properties. Previous studies reporting on the influence of alginate concentration or viscosity grade on Ca–Alg hydrogel properties generally rely on nominal viscosity classifications or limited polymer characterization [6,22,27]. In contrast, the present work provides a comprehensive hydrodynamic characterization of the alginate samples through SEC–TDA analysis that represents a key prerequisite for establishing reliable correlations between alginate molecular features and the resulting hydrogel behaviour.

Further comparisons between low- and medium-viscosity alginate samples from a different supplier (Fig. 3; Table 3) showed clear variations in hydrodynamic data, despite similar commercial labelling. This observation highlights the variability among alginate products available on the market and further emphasizes the importance of thoroughly characterizing the molecular weight distribution of the alginate used to ensure reliable and reproducible results. Since the main alginate samples used in this study were obtained from the same supplier, this approach allowed us to minimize variability associated with different alginate sources and to better isolate the effect of molecular weight and concentration. Nevertheless, the comparison with the sample from a different supplier indicates that alginates with similar nominal viscosity grades may differ substantially in their molecular

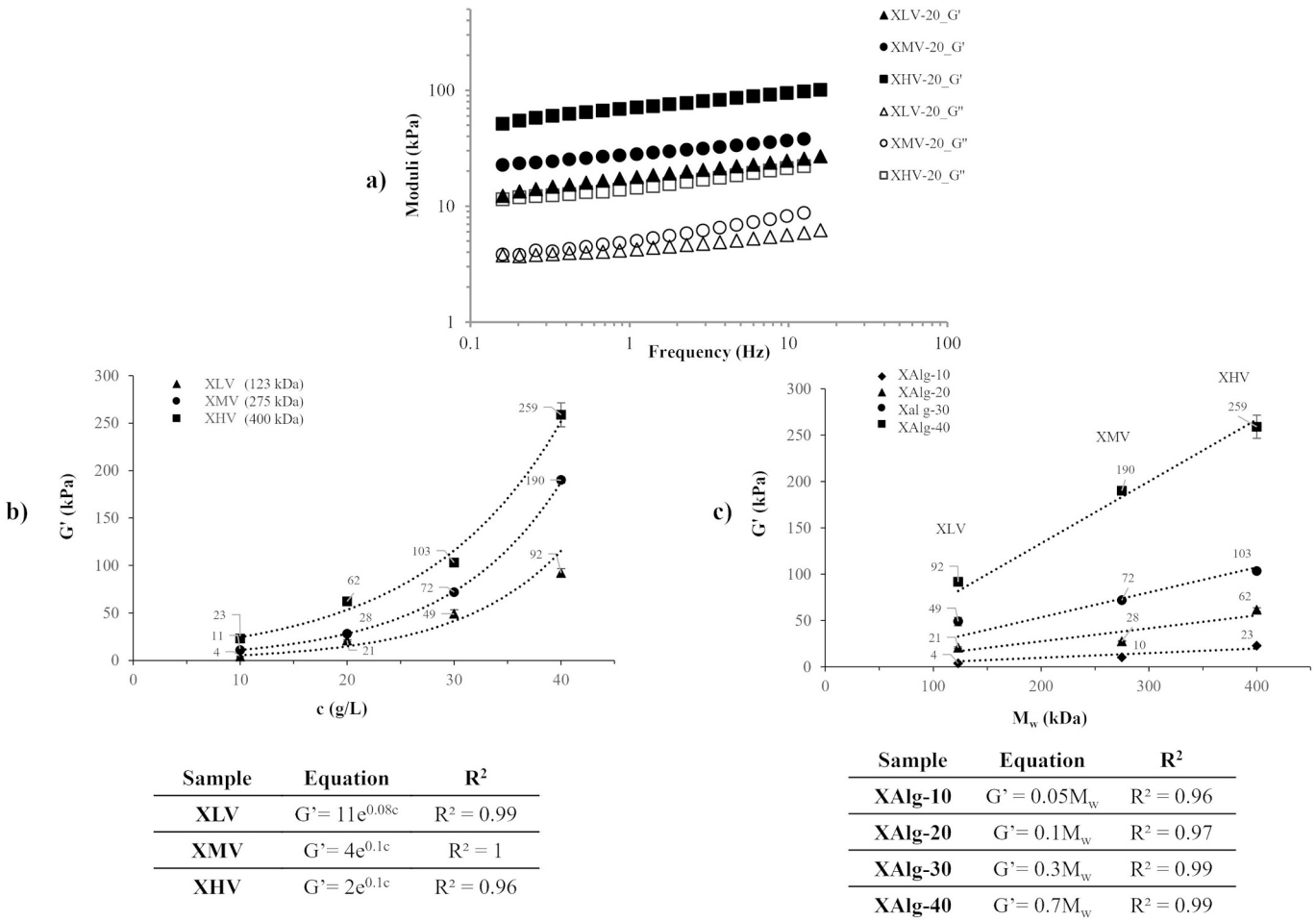

Sample	Equation	R^2
XLV	$G' = 11e^{0.08c}$	$R^2 = 0.99$
XMV	$G' = 4e^{0.1c}$	$R^2 = 1$
XHV	$G' = 2e^{0.1c}$	$R^2 = 0.96$

Sample	Equation	R^2
XAlg-10	$G' = 0.05M_w$	$R^2 = 0.96$
XAlg-20	$G' = 0.1M_w$	$R^2 = 0.97$
XAlg-30	$G' = 0.3M_w$	$R^2 = 0.99$
XAlg-40	$G' = 0.7M_w$	$R^2 = 0.99$

Fig. 7. Rheological behaviour of the sponges.
a) Representative mechanical spectra measured at a constant strain of 0.01%.
b) Correlation between storage modulus (G′) and alginate concentration.
c) Correlation between storage modulus (G′) and alginate molecular weight (M_w).
All measurements were performed on sponges equilibrated in PBS at 37 °C.

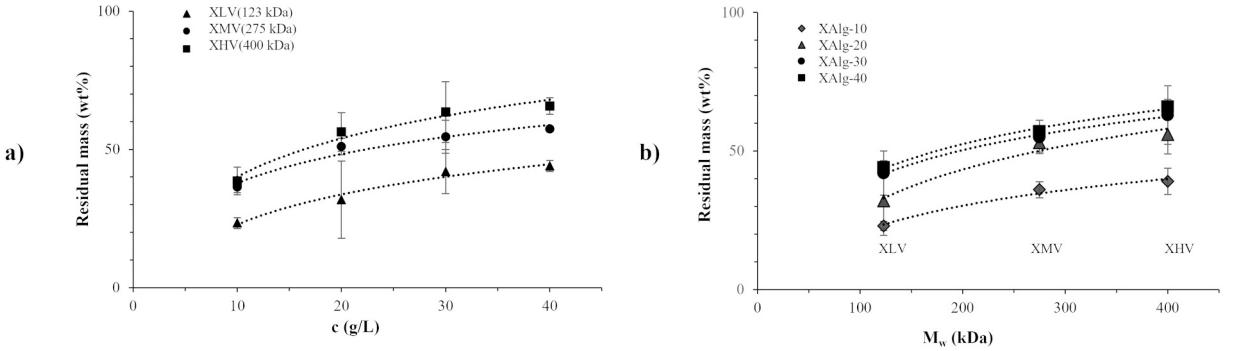

Sample	Equation	R^2
XLV	$Rm = 16\ln(c) - 13$	$R^2 = 0.97$
XMV	$Rm = 15\ln(c) + 3$	$R^2 = 0.96$
XHV	$Rm = 20\ln(c) - 6$	$R^2 = 0.97$

Sample	Equation	R^2
XAlg-10	$Rm = 14\ln(M_w) - 44$	$R^2 = 0.98$
XAlg-20	$Rm = 21\ln(M_w) - 69$	$R^2 = 0.96$
XAlg-30	$Rm = 17\ln(M_w) - 42$	$R^2 = 0.99$
XAlg-40	$Rm = 18\ln(M_w) - 44$	$R^2 = 0.99$

Fig. 8. Stability of the sponges under physiological conditions.
a) Residual mass (wt%) of alginate sponges after 30 days of incubation in PBS (pH 7.4) at 37 °C.
b) Correlation between residual mass (wt%) and alginate molecular weight (M_w, kDa); $R^2 = 0.97$.

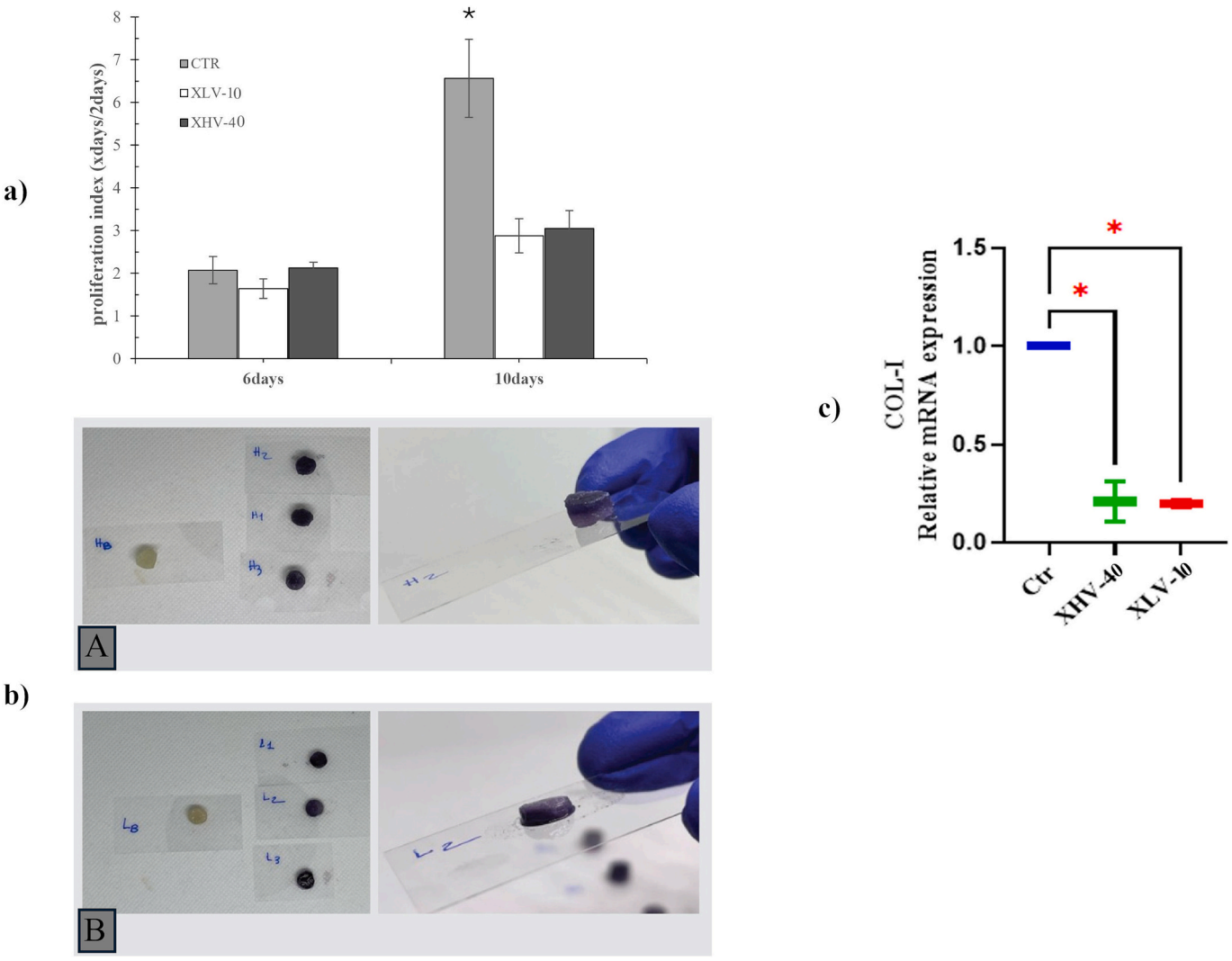

Fig. 9. Human Dermal Fibroblasts (HDFs) response to the alginate sponges.
a) MTT assay: proliferation index of HDFs after 6 and 10 days of culture. *$p < 0.01$.
b) MTT assay: representative images of the hydrogels at 24 h showing cell distribution within the different scaffolds.
c) Relative expression levels of the COL-I gene in HDFs cultured on the XAlg sponges at day 5. *$p \leq 0.05$ *vs* control.

characteristics, suggesting that some variability in hydrogel behaviour may be expected when alginates from different sources are used.

Even though Ca-Alg hydrogels are often processed into sponge-like structures *via* lyophilization, to the best of our knowledge, no previous studies have systematically investigated how alginate concentration and molecular weight affect the final sponge dimensions and density, in addition to porosity [7,8,22,39,40]. Regarding porosity, Bahrani et al. and Gong et al. reported correlations with polymer concentration, but not with molecular weight [7,22].

In this study, we demonstrated that, under our experimental conditions, these features are affected by polymer concentration more than by chain length (Fig. 4). Predictably, increasing alginate concentration leads to denser sponges. However, the effect proved less pronounced than expected: a fourfold increase in alginate concentration (from 10 g/L to 40 g/L) resulted in about only a twofold increase in sponge density. This is likely due to concentration phenomena during freezing that are more significant in less concentrated samples, as suggested by the smaller thickness recorded for the 10 g/L samples after lyophilization.

Despite the observed differences in apparent density of the sponges, no significant changes in porosity (percentage amount of void volume) were detected across the tested concentrations and molecular weights (Fig. 4c). Since the total sponge volume consists of both the polymeric fraction and the void (pore) volume, the similar porosity combined with varying apparent density suggests that the density of the polymeric fraction is lower in the 10 g/L samples. This means that a same amount of polymer occupies a larger volume in the sponges prepared at lower alginate concentrations compared to those at 40 g/L. This lower polymer density may also explain the more collapsed 3D microstructure observed in the 10 g/L samples, compared to the 40 g/L ones (Fig. 5), that is in agreement with the literature [41–44]. Among all samples tested, the high-molecular-weight alginate (HV) exhibited the most pronounced difference in 3D architecture between the 10 g/L and 40 g/L sponges, suggesting that, beyond the concentration, higher molecular weight contributes to a better morphologically defined polymeric network. This could likely arise from more cooperative (stronger) crosslinking interactions between longer polymer chains, resulting in a less deformable final network.

The high porosity values found for all the XAlg samples are in agreement with the values already reported for similar sponges [8,22]. Beyond evidencing the porous structure of the network, the morphological analyses allowed us to assess also the presence of interconnected pores, a feature key for TE applications (allowing for the diffusion of nutrients and cell by-products, cell migration and distribution across the matrix) as well as for delivery systems. The increase in pore size with

concentration is in line with the literature [43]. However, regardless of concentration and molecular weight, the pore size observed for the sponges is considered optimal for the culture of different cell types [7,8,22,45].

The water uptake capacity and mechanical behaviour of the sponges were investigated as functions of alginate molecular weight and concentration, since these properties are critical for many applications. Along with overall porosity, for instance, they influence diffusion properties within the sponges, which is essential for bioprocesses involving cells or enzymes immobilized in Ca-Alg hydrogels, as well as for biomedical applications such as drug delivery and tissue engineering. Actually, these properties govern the release kinetics of bioactive molecules entrapped within the hydrogel network and directly impact cell viability and function in tissue engineering applications. The rheological properties of the sponges are particularly relevant in tissue engineering, as they play a crucial role in regulating cell behaviour. Therefore, the ability to tune these properties would be highly desirable in view of specific intended applications.

The developed hydrogels exhibited a high swelling capacity, comparable to values reported in the literature for similar gels [28]. The positive effect of alginate concentration on the water uptake of the sponges, already reported in previous studies, was slight and observed only for the highest molecular weight tested (Fig. 6b) [6]. Similarly, a small effect of the molecular weight could be detected only at the higher concentrations employed (Fig. 6c). Overall, while these findings still point to a synergistic interaction between concentration and molecular weight, they also show that the influence of these parameters on sponge swelling is irregular, and difficult to predict. This behaviour likely arises from the interplay of multiple structural factors that affect water up-take in Ca-Alg networks. In particular, variations in apparent density and polymer-fraction density may counterbalance each other, while other parameters that strongly influence swelling, such as overall porosity and calcium amount in molar excess to alginate, remain relatively constant across the samples. As a result, the net swelling behaviour reflects the combined effect of several competing contributions rather than a single dominant parameter.

Mechanical characterization in this study was performed on sponges equilibrated in a physiological medium in the attempt to better replicate the real mechanical conditions experienced by cells (in TE applications, for instance), an aspect often overlooked in previous studies. [20]. Differently from what was observed for swelling properties, the data in Fig. 7 show that both alginate molecular weight and concentration exert significant and consistent impact on the rheological behaviour of the Ca-Alg sponges. Specifically, hydrogel stiffness increases progressively with both polymer content and chain length, according to the literature [7,8,20,22,46]. This trend aligns with the observation of a more defined/less deformed microstructure in samples with higher alginate content (reflecting a denser polymeric network) and longer polymer chains (enabling more cooperative crosslinking), as previously discussed. Notably, the relationship between stiffness and both variables follows well-defined mathematical models established under our experimental conditions. To our knowledge, this is the first systematic study providing a quantitative correlation between these key formulation parameters and the mechanical performance of calcium alginate sponges, thus allowing predictable tuning of hydrogel rigidity.

The more pronounced increase of G' with M_w observed at higher alginate concentrations further supports the synergistic effect of these two factors on hydrogel properties. Finally, considering that poor mechanical strength, particularly in the swollen state, represents a major limitation of Ca-Alg hydrogels, it is relevant that increasing alginate concentration and molecular weight produces stiffer gels while preserving both high porosity and swelling capacity, which are essential for many applications [40]. This approach overcomes conventional ones that often achieve improvement of mechanical strength at the expense of porosity and swelling, thus hindering diffusion [47].

It should be noted, however, that although the experimental design was intended to minimize variations in parameters other than those under investigation, as discussed above, the HV sample also exhibits the highest guluronic acid content (58%), which may partially contribute to its enhanced stiffness. Therefore, while the present experimental framework primarily allows the effects of molecular weight and concentration to be investigated, a complete decoupling of M_w and M/G effects would require alginate samples with independently controlled composition, which are difficult to obtain in practice for naturally derived, commercially available alginates.

Ca-Alg gels are known to lose strength and progressively solubilize in physiological environments due to competition from other ionic species (especially the abundant Na^+) for the junction sites where the G residues are complexed [48]. The rate of gel degradation must be tailored to the specific requirements of the intended application to ensure its success [48]. Our data revealed that adjusting the Alg size and c within the tested ranges, it is possible to tune the hydrogel degradation rate in physiological medium over a wide spectrum, with residual hydrogel masses recorded after 4 weeks of incubation varying from 20 to around 70 wt%. These values are compatible with most biomedical applications including TE, even when stem cells are used, as the gels remain stable long enough for cells to differentiate into the desired lineage. Results indicated that gel stability was more strongly and predictably influenced by M_w than c. While a positive correlation between alginate concentration and Ca-Alg gel stability has been previously reported [7], to our knowledge this is the first study highlighting the effect of polymer molecular weight. The observed increase in stability with higher molecular weight is likely due to stronger crosslinking between longer alginate chains, resulting from more cooperative interactions as previously discussed. In addition, longer polymer chains may promote a higher effective entanglement density and the formation of more stable cooperative junction zones between guluronic acid blocks, resulting in a more densely connected network structure.

It should be noted that the empirical relationships reported in this study were obtained under the specific experimental conditions investigated (fixed Ca^{2+} excess and sponge format) and within the tested ranges of alginate molecular weight and concentration. Consequently, extrapolation beyond these conditions should be approached with caution.

As a final part of the study, we sought to assess whether and to what extent the differences observed in the biophysical behaviour of the developed hydrogels, and depending on the parameters under investigation, impact on their performance in specific applications. To this aim, considering that this type of hydrogel is widely used for skin regeneration purposes, we tested the response of human dermal fibroblasts to the two most dissimilar hydrogels among those developed (XLV-10 and XHV-40). These two formulations were intentionally selected as representative of the most divergent physicochemical and mechanical properties obtained in this study, in order to maximize the likelihood of detecting differences in cell response. Despite the observed differences in pore size, distribution, and overall 3D microarchitecture, both sponges exhibited similarly homogeneous cell colonization (Fig. 9a). This suggests that these structural variations do not significantly affect cell infiltration, which is consistent with the macroporous nature of the sponges, all featuring pores large enough to support cell migration [39]. Moreover, the data demonstrate that both hydrogels were suitable for cell culture and, despite their significant differences in mechanical behaviour, support HDF proliferation and related collagen I expression at comparable levels. Although not necessarily expected, this outcome is particularly relevant as it indicates that higher *c* and M_w values, while improving scaffold mechanical behaviour and durability in physiological conditions, do not impair fibroblast growth or function. Notably, the stiffness of the investigated hydrogels spans a wide range (approximately 4–260 kPa), reported to influence stem cell fate, where softer matrices promote neurogenic phenotypes while stiffer substrates favour myogenic or osteogenic differentiation [49–51]. Therefore, the ability to tune hydrogel stiffness across this range through simple modulation of

Mw and polymer concentration may represent a valuable tool for designing scaffolds with application-specific mechanical properties.

Certainly, since different cell types, including stem cells, may respond differently to mechanical cues, the impact of hydrogel properties on cell fate should be carefully evaluated in application-specific contexts. For example, considering that scaffold rigidity is one of the parameters mostly affecting the fate of stem cells, it would be of great interest, in future studies, to verify whether the G′ range within which we can tune the stiffness of Ca-Alg sponges is suitable for guiding stem cell differentiation along different lineages [52]. Finally, the lower proliferative index and COLI-A1 down-regulation observed in cells cultured within the sponges, compared to the control (TCP), align with literature on fibroblast behaviour in 3D polymeric environment *vs* 2D cultures. This suggests that the sponges promote a quiescent, *in vivo*-like phenotype rather than the activated state typically induced by 2D substrates [53,54].

5. Conclusions

This study systematically investigated how alginate molecular size and concentration govern the key properties of Ca–Alg hydrogel sponges. The work advances previous work by combining full hydrodynamic characterization of alginates, which ensures reliable correlations based on rigorously defined molecular parameters, with a comprehensive evaluation of Ca–Alg hydrogel properties as a function of molecular weight and concentration, providing a robust framework for interpreting their effects on hydrogel performance and for supporting the rational design of Ca–Alg hydrogels with application-specific properties.

Based on collected data, under otherwise identical conditions, increasing alginate concentration, but not molecular weight, proved to be an effective means to increase final sponge thickness and apparent density, albeit to a lesser extent than expected, while porosity remained consistently high. Morphological observations further suggested that both alginate chain length and concentration synergistically contributed to a well-defined three-dimensional microarchitecture. Conversely, varying alginate molecular weight and concentration proved ineffective in consistently modulating water uptake, indicating that simultaneous adjustment of multiple parameters, or manipulation of other factors held constant in this study, may be necessary.

Notably, both alginate molecular weight and concentration proved powerful levers to fine-tune mechanical stiffness and stability in physiological environments, two critical and often challenging features of Ca–Alg hydrogels. This is the first study to provide quantitative relationships correlating these properties to alginate molecular parameters, offering a predictive and practical framework for rational hydrogel design. Biological evaluation, using human dermal fibroblasts, demonstrated that enhanced mechanical performance and stability can be achieved by adjusting polymer M_w and *c*, without compromising key aspects of cell response, including homogeneous colonization, proliferation and function, representing an advance over prior approaches. Moreover, these findings may inform the design of systems in which increased hydrogel stiffness could be exploited to influence stem cell behaviour and, potentially, guide differentiation.

Overall, this study provides valuable insight into how and to what extent alginate M_w and *c* influence final hydrogel behaviour, offering a robust and predictive framework for tailoring Ca–Alg hydrogels to specific applications.

CRediT authorship contribution statement

Sabrina Cuomo: Writing – original draft, Validation, Methodology, Investigation, Formal analysis, Data curation. **Francesca Rispo:** Writing – original draft, Visualization, Validation, Methodology, Investigation, Formal analysis, Data curation. **Bartolomeo Coppola:** Writing – original draft, Visualization, Validation, Methodology, Investigation, Formal analysis, Data curation. **Emiliano Bedini:** Writing – original draft, Visualization, Validation, Methodology, Investigation, Formal analysis, Data curation. **Maria D'Agostino:** Writing – original draft, Visualization, Validation, Methodology, Formal analysis, Data curation. **Elisabetta Cassese:** Writing – original draft, Visualization, Validation, Methodology, Formal analysis, Data curation. **Paola Palmero:** Writing – review & editing, Writing – original draft, Visualization, Validation. **Chiara Schiraldi:** Writing – review & editing, Visualization, Validation, Resources, Funding acquisition. **Annalisa La Gatta:** Writing – review & editing, Writing – original draft, Visualization, Validation, Supervision, Project administration, Methodology, Data curation, Conceptualization.

Funding

This work was partially supported by the MIMIT project "CROSS-GaG" CUP B29J24001220005 (Italy). Dr. Sabrina Cuomo is enrolled in an industrial PhD program partially funded by IBSA Italia.

Declaration of competing interest

The authors declare that they have no known competing financial interests or personal relationships that could have appeared to influence the work reported in this paper.

Appendix A. Supplementary data

Supplementary data to this article can be found online at https://doi.org/10.1016/j.ijbiomac.2026.151578.

Data availability

Data will be made available on request.

References

[1] C. Peteiro, Alginate production from marine macroalgae, with emphasis on kelp farming, in: B.H.A. Rehm, M.F. Moradali (Eds.), Alginates and Their Biomedical Applications, Springer, Singapore, 2017, pp. 27–66.
[2] F. Clementi, Alginate production by Azotobacter vinelandii, Crit. Rev. Biotechnol. 17 (1997) 327–361, https://doi.org/10.3109/07388559709146618.
[3] N. Kaur, B. Singh, S. Sharma, Hydrogels for potential food application: effect of sodium alginate and calcium chloride on physical and morphological properties, Pharma Innov. J. 7 (2018) 142–148.
[4] Y. Ren, Q. Wang, W. Xu, M. Yang, W. Guo, S. He, et al., Alginate-based hydrogels mediated biomedical applications: a review, Int. J. Biol. Macromol. 279 (2024) 135019, https://doi.org/10.1016/j.ijbiomac.2024.135019.
[5] L. Li, B. Zhu, Z. Yao, J. Jiang, Directed preparation, structure–activity relationship and applications of alginate oligosaccharides with specific structures: a systematic review, Food Res. Int. 170 (2023) 112990, https://doi.org/10.1016/j.foodres.2023.112990.
[6] B. Enobakhare, D.L. Bader, D.A. Lee, Concentration and M/G ratio influence the physiochemical and mechanical properties of alginate constructs for tissue engineering, J. Appl. Biomater. Funct. Mater. 4 (2006) 87–96, https://doi.org/10.1177/228080000600400203.
[7] N. Bahrami, A. Farzin, F. Bayat, A. Goodarzi, M. Salehi, R. Karimi, A. Mohamadnia, A. Parhiz, J. Ai, Optimization of 3D alginate scaffold properties with interconnected porosity using freeze-drying method for cartilage tissue engineering application, Arch. Neurosci. 6 (2019) e85122, https://doi.org/10.5812/ans.85122.
[8] F. de la Portilla, S. Pereira, M. Molero, F. De Marco, V. Perez-Puyana, A. Guerrero, A. Romero, Microstructural, mechanical, and histological evaluation of modified alginate-based scaffolds, J. Biomed. Mater. Res. A 104 (2016) 3107–3114, https://doi.org/10.1002/jbm.a.35857.
[9] L. Luo, Y. Gong, L. Yan, Y. Bu, Sponge as scaffolds in bone and cartilage tissue engineering, Chem. Res. Chin. Univ. 40 (2024) 786–797, https://doi.org/10.1007/s40242-024-4135-0.
[10] J. Jang, H. Kim, Y. Kim, J. Park, Effects of alginate hydrogel cross-linking density on mechanical and biological behaviors for tissue engineering, J. Mech. Behav. Biomed. Mater. 37 (2014) 69–77, https://doi.org/10.1016/j.jmbbm.2014.05.004.
[11] A. Serafin, M. Culebras, M.N. Collins, Synthesis and evaluation of alginate, gelatin, and hyaluronic acid hybrid hydrogels for tissue engineering applications, Int. J. Biol. Macromol. 233 (2023) 123438, https://doi.org/10.1016/j.ijbiomac.2023.123438.
[12] Y. Yuan, M. Yin, L. Chen, F. Liu, M. Chen, F. Zhong, Effect of calcium ions on the freeze-drying survival of probiotic encapsulated in sodium alginate, Food Hydrocoll. 130 (2022) 107668, https://doi.org/10.1016/j.foodhyd.2022.107668.

[13] S. Parvez, I.A. Wani, Calcium alginate beads loaded with green tea extract: impact of drying methods on its structure, release behavior, and storage stability, ACS Food Sci. Technol. 4 (2024) 935–946, https://doi.org/10.1021/acsfoodscitech.3c00696.
[14] L. Xia, X. Luo, Y. Zhu, X. Zhang, L. Luo, Effects of $CaCl_2$ freeze-drying and acidic solutions on the reusability of calcium alginate beads; and degradation of phenol by immobilized Acinetobacter sp. PR1, Biochem. Eng. J. 151 (2019) 107339, https://doi.org/10.1016/j.bej.2019.107339.
[15] K.M. Manjanna, T.M. Pramod Kumar, B. Shivakumar, Calcium alginate cross-linked polymeric microbeads for oral sustained drug delivery in arthritis, Drug Discov. Ther. 4 (2010) 109–122.
[16] K. Essifi, M. Brahmi, D. Berraaouan, A. Ed-Daoui, A. El Bachiri, M.L. Fauconnier, A. Tahani, Influence of sodium alginate concentration on microcapsules properties foreseeing the protection and controlled release of bioactive substances, J. Chem. (2021) 5531479, https://doi.org/10.1155/2021/5531479.
[17] H. Wang, S. Huang, X. Xu, Calcium alginate reinforced zwitterionic double network hydrogel with mechanical robustness and antimicrobial activity for freshwater shrimp spoilage detection, Food Res. Int. 115483 (2025), https://doi.org/10.1016/j.foodres.2024.115483.
[18] X. Xu, pH-responsive fluorescent hydrogels for food anticounterfeiting, freshness monitoring and preservation: mechanisms, fabrication strategies, and emerging applications, Trends Food Sci. Technol. 105499 (2025), https://doi.org/10.1016/j.tifs.2025.105499.
[19] H.J. Kong, K.Y. Lee, D.J. Mooney, Decoupling the dependence of rheological/mechanical properties of hydrogels from solids concentration, Polym 43 (2002) 6239–6246, https://doi.org/10.1016/S0032-3861(02)00559-1.
[20] M.A. LeRoux, F. Guilak, L.A. Setton, Compressive and shear properties of alginate gel: effects of sodium ions and alginate concentration, J. Biomed. Mater. Res. 47 (1999) 46–53, https://doi.org/10.1002/(SICI)1097-4636(199910)47:1<46::AID-JBM6>3.0.CO;2-N.
[21] M. Matyash, F. Despang, C. Ikonomidou, M. Gelinsky, Swelling and mechanical properties of alginate hydrogels with respect to promotion of neural growth, Tiss. Eng. Part C: Methods 20 (2014) 401–411, https://doi.org/10.1089/ten.tec.2013.025.
[22] Y. Gong, G.T. Han, Y.M. Zhang, J.F. Zhang, W. Jiang, X.W. Tao, S.C. Gao, Preparation of alginate membrane for tissue engineering, J. Polym. Eng. 36 (2016) 363–370, https://doi.org/10.1515/polyeng-2015-0065.
[23] S.L. Tomić, M.M. Babić Radić, J.S. Vuković, V.V. Filipović, J. Nikodinovic-Runic, M. Vukomanović, Alginate-based hydrogels and scaffolds for biomedical applications, Mar. Drugs 21 (2023) 177, https://doi.org/10.3390/md21030177.
[24] H. Wang, L. Yang, Y. Yang, A review of sodium alginate-based hydrogels: structure, mechanisms, applications, and perspectives, Int. J. Biol. Macromol. 292 (2025) 139151, https://doi.org/10.1016/j.ijbiomac.2024.139151.
[25] K.Y. Lee, D.J. Mooney, Alginate: properties and biomedical applications, Polym. Sci. 37 (2012) 106–126, https://doi.org/10.1016/j.progpolymsci.2011.06.003.
[26] C. Bennacef, S. Desobry, J. Jasniewski, S. Leclerc, L. Probst, S. Desobry-Banon, Influence of alginate properties and calcium chloride concentration on alginate bead reticulation and size: a phenomenological approach, Polym 15 (2023) 4163, https://doi.org/10.3390/polym15204163.
[27] P.M. Bohari, Siti, D.W.L. Hukins, L.M. Grover, Effect of calcium alginate concentration on viability and proliferation of encapsulated fibroblasts, Biomed. Mater. Eng. 21 (2011) 159–170, https://doi.org/10.3233/BME-2011-0665.
[28] I.M. Savić Gajić, I.M. Savić, Z. Svirčev, Preparation and characterization of alginate hydrogels with high water-retaining capacity, Polym 15 (2023) 2592, https://doi.org/10.3390/polym15122592.
[29] J. Zhang, E. Wehrle, J.R. Vetsch, G.R. Paul, M. Rubert, R. Müller, Alginate dependent changes of physical properties in 3D bioprinted cell-laden porous scaffolds affect cell viability and cell morphology, Biomed. Mater. 14 (2019) 065009, https://doi.org/10.1088/1748-605X/ab3c74.
[30] P. Duan, N. Kandemir, J. Wang, J. Chen, Rheological characterization of alginate-based hydrogels for tissue engineering, MRS Adv. 24 (2017) 1309–1314, https://doi.org/10.1557/adv.2017.8.
[31] C.K. Kuo, P.X. Ma, Maintaining dimensions and mechanical properties of ionically crosslinked alginate hydrogel scaffolds in vitro, J. Biomed. Mater. Res. Part A 84 (84) (2018) 899–907, https://doi.org/10.1002/jbm.a.31375.
[32] F.E. Freeman, D.J. Kelly, Tuning alginate bioink stiffness and composition for controlled growth factor delivery and to spatially direct MSC fate within bioprinted tissues, Sci. Rep. 7 (2017) 17042, https://doi.org/10.1038/s41598-017-17286-1.
[33] P.A. Williams, K.T. Campbell, E.A. Silva, Alginate hydrogels of varied molecular weight distribution enable sustained release of sphingosine-1-phosphate and promote angiogenesis, J. Biomed. Mater. Res. Part A 106 (2018) 138–146, https://doi.org/10.1002/jbm.a.36217.
[34] A. La Gatta, I. Marzaioli, M. De Rosa, C. Schiraldi, A complete hyaluronan hydrodynamic characterization using a triple detector-SEC system during in vitro enzymatic degradation, Anal. Biochem. 404 (2010) 21–29, https://doi.org/10.1016/j.ab.2010.04.014.
[35] A. Theisen, C. Johann, M.P. Deacon, S.E. Harding, Refractive Increment Dat-Book, Nottingham University Press, Nottingham, 1999.
[36] F. Barrino, V. Vassallo, M. Cammarota, M. Lepore, M. Portaccio, C. Schiraldi, A. La Gatta, A comprehensive in vitro characterization of non-crosslinked, diverse tissue-derived collagen-based membranes intended for assisting bone regeneration, PLoS One 19 (2024) e0298280, https://doi.org/10.1371/journal.pone.0298280.
[37] L. Sartore, C. Manferdini, Y. Saleh, K. Dey, E. Gabusi, G. Ramorino, G. Lisignoli, Polysaccharides on gelatin-based hydrogels differently affect chondrogenic differentiation of human mesenchymal stromal cells, Mater. Sci. Eng. C 126 (2021) 112175, https://doi.org/10.1016/j.msec.2021.112175.
[38] H. Grasdalen, High-field, 1H-n.m.r. spectroscopy of alginate: sequential structure and linkage conformations, Carbohydr. Res. 118 (1983) 255–260, https://doi.org/10.1016/0008-6215(83)88053-7.
[39] L. Shapiro, Lilia, S. Cohen, Novel alginate sponges for cell culture and transplantation, Biomater 18 (1997) 583–590, https://doi.org/10.1016/S0142-9612(96)00181-0.
[40] W. Hu, J. Zhang, Y. Xia, Y. Gao, Y. Zhao, Green and facile fabrication of robust calcium alginate sponges via thermally bonded nonwoven induced freeze-drying for dressing applications, Colloids Surf. A Physicochem. Eng. Asp. 697 (2024) 134342, https://doi.org/10.1016/j.colsurfa.2024.134342.
[41] A. Serafin, M. Culebras, M.N. Collins, Synthesis and evaluation of alginate, gelatin, and hyaluronic acid hybrid hydrogels for tissue engineering applications, Int. J. Biol. Macromol. 233 (2023) 123438, https://doi.org/10.1016/j.ijbiomac.2023.123438.
[42] M. Antonietti, R.A. Caruso, C.G. Göltner, M.C. Weissenberger, Morphology variation of porous polymer gels by polymerization in lyotropic surfactant phases, Macromol 32 (1999) 1383–1389, https://doi.org/10.1021/ma9812478.
[43] A.A. Solbu, A. Koernig, J.S. Kjesbu, D. Zaytseva-Zotova, M. Sletmoen, B.L. Strand, High resolution imaging of soft alginate hydrogels by atomic force microscopy, Carbohydr. Polym. 276 (2022) 118804, https://doi.org/10.1016/j.carbpol.2021.118804 (Get rights and content).
[44] P.N. Dave, A. Gor, Natural polysaccharide-based hydrogels and nanomaterials: recent trends and their applications, in: M. Mustansar Hussain (Ed.), Handbook of Nanomaterials for Industrial Applications, Elsevier, Amsterdam, 2018, pp. 36–66, https://doi.org/10.1016/B978-0-12-813351-4.00003-1.
[45] I. Bružauskaitė, D. Bironaitė, E. Bagdonas, E. Bernotienė, Scaffolds and cells for tissue regeneration: different scaffold pore sizes—different cell effects, Cytotechnol 68 (2016) 355–369, https://doi.org/10.1007/s10616-015-9895-4.
[46] G. Kaklamani, D. Cheneler, L.M. Grover, M.J. Adams, J. Bowen, Mechanical properties of alginate hydrogels manufactured using external gelation, J. Mech. Behav. Biomed. Mater. 36 (2014) 135–142, https://doi.org/10.1016/j.jmbbm.2014.04.013.
[47] A. Hurtado, A.A. Aljabali, V. Mishra, M.M. Tambuwala, A. Serrano-Aroca, Alginate: enhancement strategies for advanced applications, Int. J. Mol. Sci. 23 (2022) 4486, https://doi.org/10.3390/ijms23094486.
[48] D. Shahriari, J. Koffler, D.A. Lynam, M.H. Tuszynski, J.S. Sakamoto, Characterizing the degradation of alginate hydrogel for use in multilumen scaffolds for spinal cord repair, J. Biomed. Mater. Res. Part A 104 (2016) 611–619, https://doi.org/10.1002/jbm.a.35600.
[49] A.J. Engler, S. Sen, H.L. Sweeney, D.E. Discher, Matrix elasticity directs stem cell lineage specification, Cell 126 (2006) 677–689, https://doi.org/10.1016/j.cell.2006.06.044.
[50] K.H. Vining, D.J. Mooney, Mechanical forces direct stem cell behaviour in development and regeneration, Nat. Rev. Mol. Cell Biol. 18 (2017) 728–742, https://doi.org/10.1038/nrm.2017.108.
[51] D.E. Discher, P. Janmey, Y.L. Wang, Tissue cells feel and respond to the stiffness of their substrate, Sci 310 (2005) 1139–1143, https://doi.org/10.1126/science.1116999.
[52] H.J. Kong, T.R. Polte, E. Alsberg, D.J. Mooney, FRET measurements of cell-traction forces and nano-scale clustering of adhesion ligands varied by substrate stiffness, Proc. Natl. Acad. Sci. 102 (2005) 4300–4305, https://doi.org/10.1073/pnas.0405873102.
[53] J.P. Woodley, D.W. Lambert, I.O. Asencio, Reduced fibroblast activation on electrospun polycaprolactone scaffolds, Bioeng 10 (2023) 348, https://doi.org/10.3390/bioengineering10030348.
[54] N. Migulina, R.H. de Hilster, S. Bartel, R.H. Vedder, M. van den Berge, A. Nagelkerke, J. K., W. Timens, M.C. Harmsen, M.N. Hylkema, C.-A. Brandsma, 3-D culture of human lung fibroblasts decreases proliferative and increases extracellular matrix remodeling genes, Am. J. Physiol.-Cell Physiol. 326 (2024), https://doi.org/10.1152/ajpcell.00374.2023.